EDGE ARTICLE

Check for updates

All publication charges for this article have been paid for by the Royal Society of Chemistry

Learning the structure–activity relationship (SAR) of the Wittig reaction from genetically-encoded substrates†

Kejia Yan,[a] Vivian Triana,[a] Sunil Vasu Kalmady,[b] Kwami Aku-Dominguez,[a] Sharyar Memon,[c] Alex Brown, [a] Russell Greiner[bd] and Ratmir Derda [*a]

The Wittig reaction can be used for late stage functionalization of proteins and peptides to ligate glycans, pharmacophores, and many other functionalities. In this manuscript, we modified 160 000 N-terminal glyoxaldehyde peptides displayed on phage with the Wittig reaction by using a biotin labeled ylide under conditions that functionalize only 1% of the library population. Deep-sequencing of the biotinylated and input populations estimated the rate of conversion for each sequence. This "deep conversion" (DC) from deep sequencing correlates with rate constants measured by HPLC. Peptide sequences with fast and slow reactivity highlighted the critical role of primary backbone amides (N–H) in accelerating the rate of the aqueous Wittig reaction. Experimental measurement of reaction rates and density functional theory (DFT) computation of the transition state geometries corroborated this relationship. We also collected deep-sequencing data to build structure–activity relationship (SAR) models that can predict the DC value of the Wittig reaction. By using these data, we trained two classifier models based on gradient boosted trees. These classifiers achieved area under the ROC (receiver operating characteristic) curve (ROC AUC) of 81.2 ± 0.4 and 73.7 ± 0.8 (90–92% accuracy) in determining whether a sequence belonged to the top 5% or the bottom 5% in terms of its reactivity. This model can suggest new peptides never observed experimentally with 'HIGH' or 'LOW' reactivity. Experimental measurement of reaction rates for 11 new sequences corroborated the predictions for 8 of them. We anticipate that phage-displayed peptides and related mRNA or DNA-displayed substrates can be employed in a similar fashion to study the substrate scope and mechanisms of many other chemical reactions.

Introduction

Profiling multiple substrates under the same reaction conditions is a cornerstone of mechanistic organic chemistry. Optimization of chemical reactions, discovery of catalytic systems, and mechanistic studies are based on measurements of reaction rates of multiple substrates and conditions, and all these situations need a more efficient way to select the right substrates from a large number of compounds. The data collected in such structure–activity relationship (SAR) studies serve as an essential input for developing mechanistic hypotheses and decision making in the discovery of new reactions, however, measurement of the rates of a plurality of substrates

under different reaction conditions one-by-one is time consuming.[1] Quantitative analyses starting from the pioneering work of Hammett and co-workers on linear free energy relationships (LFER)[2] to modern approaches that employ multiple linear regression (MLR)[3] and other machine learning (ML) methods[4] permit converting observations from SAR studies to quantitative models that relate reactivity to observable physical properties such as pK_a or theoretically calculated parameters such as HOMO/LUMO energies. These models, combined with "qualitative chemical intuition," allow prediction of optimal conditions and substrates for a particular reaction and provide critical insight into reaction mechanisms. The most valuable input for these models consists of both "positive" and "negative" data (*i.e.*, fast and slow reactions). The same requirements exist in other machine learning fields: sets with positive and negative observations serve as the most effective input for the training of models.[5–7] Methods that allow collection of a large unbiased set of reactivity data facilitate building models that minimize the bias that could originate from human decision making such as conscious selection of substrates with anticipated reactivity.

a Department of Chemistry, University of Alberta, Edmonton, AB T6G 2G2, Canada. E-mail: ratmir@ualberta.ca

b Department of Computer Science, University of Alberta, Alberta, AB T6G 2E8, Canada

c Department of Electrical and Computer Engineering, University of Alberta, Edmonton, AB T6G 1H9, Canada

d Alberta Machine Intelligence Institute, Alberta, AB T5J 3B1, Canada

The high-throughput screening (HTS) technique was developed in the early 1990s for the discovery of pharmaceutically valuable molecules.[8,9] It was later repurposed for high-throughput acquisition of SAR information. Such HTS approaches have facilitated not only optimization of chemical reactions[10] but also discovery of catalytic systems,[11–14] and unexpected chemical transformations.[9] Screening of a mixture of multiple substrates in one solution[15] expands the traditional one-well-one-reaction format.[9,16] Multisubstrate screening[17,18] can evaluate yields and enantiomeric excesses for multiple substrates converted by a catalyst,[19] and determine reaction kinetics and corresponding rate constants of a large number of reactions in a few experiments (340 measurements in 17 experiments),[20] and it can be used to discover new transformations. Traditional considerations in multisubstrate approaches are throughput and non-linearity. The complexity of the mixture should be amenable to separation by liquid or gas chromatography (LC or GC) and the concentration of individual substrates should be sufficiently high to permit the analysis by mass-spectrometry (MS). However, if substrates are present at high concentrations, nonlinear effects[21] may originate in such mixtures due to the cross-reactivity between multiple substrates and products. Genetically-encoded (GE) peptide libraries[9,16] and DNA-encoded small molecule libraries (DEL)[22–26] associate the DNA message with each substrate, and this message can be amplified from a single copy number. This amplification makes it possible to perform screening at very low concentrations of substrates. In term low concentration minimizes undesired cross-substrate reactions (Fig. S2†) while conveniently increasing the number of substrates that can be interrogated to 10^6–10^{12} scale. In this manuscript, we perform multisubstrate screening using >10^5 genetically-encoded substrates present in one solution at 10 attomolar/substrate concentration and employ deep-sequencing to monitor the reactions. Such a concentration of substrates minimizes the interaction between the substrates and can be used to collect valuable information to understand the SAR of the Wittig reaction.

Phage display and DEL technology have been successfully applied to discover new reactions.[22–24,26–29] A traditional application of DEL or GE-peptide libraries in reaction discovery aims to enrich a rare subset of substrates that exhibit a faster reactivity than the average population. Such an approach can be broadly characterized as a "gain of function" screen. Knowledge emanating from the screenings focused on "gain" in chemical reactivity is insufficient for comprehensive structure–activity models. The problem can be easily resolved if the genetically-encoded screening is modified to identify both "gain" and "loss" of function in chemical reactivity. Here we demonstrate modification of GE-libraries under kinetically-controlled conditions that convert ~1% of the library and deep-sequencing of the modified population identified both the fast and slow-reacting substrates. We implement such a GE-screening to identify the peptides that increase and decrease the rate of the Wittig reaction in water and then train the dataset use machine learning to predict peptide reactivity.

The Wittig reaction is a versatile and biocompatible carbon–carbon bond forming process; the product of the reaction can serve as a versatile electrophile or dienophile building block, or as a warhead for reversible covalent trapping of biological nucleophiles. The Wittig reaction has been employed to synthesize DNA-encoded libraries and modify phage displayed libraries of aldehyde-peptides.[30,31] The substrates for the Wittig reaction—libraries of peptide aldehydes have been generated by $NaIO_4$ oxidation of readily available phage-displayed libraries with N-terminal Ser.[32–34] Aldehydes can also be introduced by unnatural amino acid mutagenesis[35] or by using formyl glycine generating enzymes.[36] The mechanism of the Wittig reaction in water remains a topic of extensive research.[37–39] It proceeds through a formal cycloaddition with an early oxaphosphetane (OPA) transition state (TS). The stereo-electronic properties of the aldehydes influence the geometry and energy around the OPA manifold and change the rate and stereo chemical outcome of the Wittig reaction. Peptide aldehyde substrates contain a rich repertoire of functional groups that could potentially stabilize or destabilize the OPA TS. The effect of hydroxyl groups with pK_a of 7–15, ammonium ions with pK_a 7–12, carboxylates, aromatic rings with different "π-basicity" and different H-bond donors and acceptors on the stability of OPA in water is not obvious. The GE-screen described in this report profiled the effect of a diverse combination of these groups in 10^5 peptide-aldehydes displayed on phage. The predictions built on these observations illustrated the unique role of primary amides in stabilizing the transition state *via* short-range non-covalent interactions.

Results and discussion

Wittig reaction in the linear phage library

Multisubstrate profiling of the Wittig reaction repurposed classical tagging strategies employed for physical separation of the reacted subset of library members from the remaining unreacted population.[32,40] In particular, successful Wittig reaction between phage-displayed peptide-aldehydes and biotin-tagged ylides introduced biotin into a product. Tagged products can be separated from the unreacted population due to its affinity to streptavidin and analyzed by deep-sequencing. We employed periodate oxidation[32] of linear SXXXX libraries displayed on phage[41] to produce libraries of aldehyde substrates denoted as CHO–XXXX (Fig. 1a, X denotes any of the 20 amino acids). The resulting library of $(20)^4 = 160\ 000$ substrates can be characterized completely by Illumina sequencing (Fig. 1).[41] Change in the library composition that leads to either enrichment or depletion of substrates in these libraries can be, therefore, reliably quantified.

Based on previously reported average rates of the reaction on phage ($k = 0.2\ \text{M}^{-1}\ \text{s}^{-1}$),[31] a 10 minute reaction time and 0.4 mM ylide ester biotin (YEB) should convert ~5% of the population to a biotinylated product (Fig. S2†). Kinetic modeling of the distribution of the products in the multisubstrate reaction predicts that interrupting the reaction at 5% conversion of the aldehyde population and counting the copy number of the biotinylated products make it possible to identify substrates with rates that range from 0.002 $\text{M}^{-1}\ \text{s}^{-1}$ to 20 $\text{M}^{-1}\ \text{s}^{-1}$ (Fig. S1d†). Therefore, interruption of the reaction at 1–5%
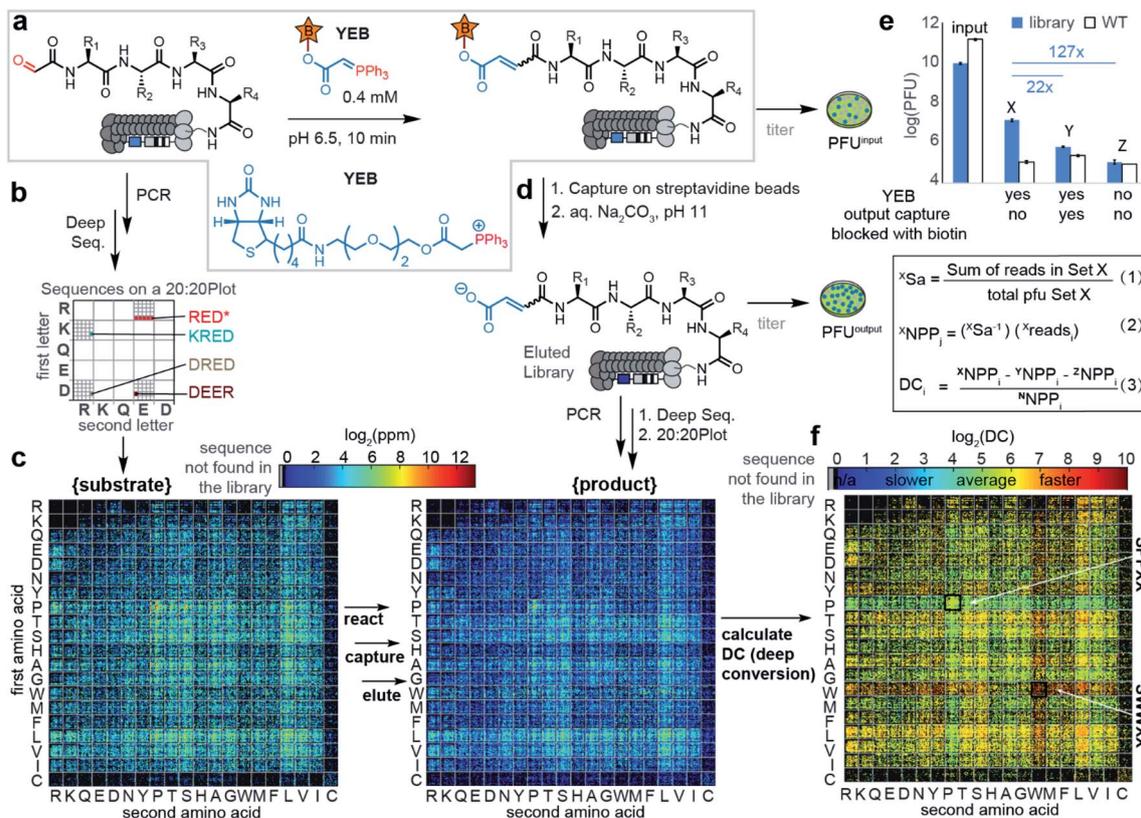
Fig. 1 (a) Wittig reaction on phage libraries. PFU is a plaque-forming unit. (b) Reading of a 20 × 20 plot.[41] (c) 20 × 20 plots displaying library-wide DC values of peptide substrates and the Wittig products. Black pixels in the 20 × 20 plot correspond to sequences not observed during sequencing. (d) After reacting for 10 min, the biotinylated Wittig products were captured by streptavidin beads and subjected to sequencing. (e) Pull-down titering data showing higher capture of phage expressing peptides (blue bars) *vs.* wild type phage (white bars) and higher capture in the 1% biotinylated set (*X*) than in controls (*Y* and *Z*). To calculate the deep conversion of a particular peptide "*i*" (DC_i), we calculate the number of phage particles (NPP_i) that display peptides using deep sequencing number of reads ($reads_i$) observed in the deep sequencing and sampling factor (S_a) that relates reads in deep sequencing ($reads_i$) with NPP_i. The detailed description of eqn (1)–(3) is provided in Scheme S1.† (f) 20 × 20 plots for SX_4 selections. Plots with amino acids at other positions can be found in Fig. S3.†

conversion should make it possible to identify substrates that react 100 times faster or 100 times slower than the average substrate. Adding these pre-determined concentrations of YEB to 10^9 phage virions and quenching with acidic buffer at the specified time intervals, ensured reproducible biotinylation of ∼1% of the population of phage clones.

The pull-down process selects not only the "specific" biotinylated population but also the peptide sequences that bind non-specifically to the components in the system such as protein streptavidin agarose beads. A set of two controls assessed the magnitude of such non-specific binding to be 1–5% of the specific biotin-streptavidin interaction. Recovery of biotinylated peptides by streptavidin blocked biotin-binding sites (set *Y*, Fig. 1e) and recovery of the unreacted aldehyde-peptide population by streptavidin (set *Z*, Fig. 1e) was decreased by factors of 22 and 120 when compared to the recovery of the "specific" population (set *X*, Fig. 1e). We collected these "specific" and control populations in 3–5 independent experiments, and subjected them to PCR and Illumina sequencing. The combined data were used to identify the normalized copy number of the peptides that were biotinylated during the Wittig

reaction (Fig. 1d and S2,† all the sequencing data are available in the ESI also as http://VT_unfiltered_Feb.txt).

Fig. 1e and Scheme S1† summarize the calculations of the absolute number of biotinylated particles from sequencing data accounting for factors like the sequencing depth and amount of phage particles in each specific experiment. "N_i" (copy number of the peptide in the naïve library) was critical to account for sequences that were present in a high copy number in naïve libraries but did not react fast in the Wittig reaction. Applying normalization and sampling correction (S_a) to peptide sequences, values denoted as "Deep Conversion" (DC) for over 50 000 peptide aldehyde sequences were generated (all the DC values are available in http://MLinput.txt). The DC values are conceptually related to reactivities of sequences: the higher the DC value, the more reactive is the peptide. We found that the most straightforward approach for observing the relation between the sequence and conversion was by using a library-wide visualization tool referred to as the "20 × 20 plot" used in our previous studies (Fig. 1f and S3†).[41] To illustrate the importance of normalization in calculation of DC values, we noted that biotin-tagged SPPXX sequences were observed in

high copy numbers in captured population and they can be mistakenly interpreted as "most reactive" substrates (Fig. 1c). On the other hand, these sequences were also present in high copy numbers in the naïve library (Fig. 1c) and the introduction of normalization predicted that SPPXX sequences in fact have the lowest DC values in the Wittig reaction (Fig. 1f).

To confirm that the observations predicted by high and low deep conversion (DC) indeed correlated with experimentally determined reactivities of peptide aldehydes, we selected a series of peptides predicted to be "fast", "medium" and "slow", synthesized them and validated the reaction rate (Fig. S4–S6†). The results showed an agreement between the experimentally determined conversion measured by HPLC and DC (Fig. 2) in the range of two orders of magnitude for both values. In particular, we reported previously that the average rate for the library of peptide aldehydes displayed on phage was 0.23 ± 0.09 M^{-1} s^{-1}.[31] This rate constant was similar to the rate constant for "average" synthetic peptide sequences that did not contain Trp or Pro residues in the first two positions (Fig. 2a). In contrast, synthetic aldehydes HCO–PPLA and HCO–PPPL exhibited rates of 0.017 ± 0.005 and 0.014 ± 0.03 M^{-1} s^{-1} respectively. These sequences were up to 13–16-fold slower than that of the average population. This observation was in line with the observed decrease in DC for SPPXX sequences highlighted by using the 20×20 plot (Fig. 1f). To test the effect of proline in a specific position, we systematically evaluated the reactivity of HCO–PPPA, HCO–PPAA, HCO–PAAA, HCO–APAA and HCO–AAAP sequences (Fig. 2a and S9,† all the peptide traces can be found in Fig. S31–S50†). Replacing either the 1st or 2nd amino acid with proline leads only to a modest 2–3 fold decrease in the rate whereas simultaneous replacement of the 1st and 2nd amino acids with prolines resulted in a 10-fold decrease. Subsequent introduction of proline in the 3rd or 4th position

had little additional effect on the rate of the Wittig reaction. In analysis of HCO–PXXX sequences, we observed a known side reaction that consumed HCO–PXXX aldehydes via proline-assisted 6-exo-trig attack of an amide nitrogen on the aldehyde (Fig. S10†).[42] In HPLC assay, the rate of the Wittig reaction for HCO–PXXX was measured to be 0.12–0.17 M^{-1} s^{-1} and the rates of cyclization were in a similar range. Combination of both processes as can be seen in the kinetic equation in Fig. 2b, contributed to an apparent decrease in DC. We also examined the factors that led to an increase in DC and focused on peptides with tryptophan in the first and second positions. The introduction of only one tryptophan in peptides HCO–QWLH, HCO–WIVR, HCO–HWFP, HCO–LWYR and HCO–WLPR (Fig. 2a) had no statistically significant increase from average reactivity, whereas sequences HCO–WWPQ and HCO–WWGL with two tryptophan residues in both positions, exhibited significant increases from the average rate and more than 50-fold increase from the lowest rate in the population. These results suggested that the first and second N-terminal amino acids play a critical synergistic role in the rate of the Wittig reaction, possibly by stabilizing or destabilizing the OPA TS. These observations also confirmed that DC values serve as a good predictive surrogate for fast and slow reactions.

Investigation of the transition states of the Wittig reaction

Proline, unlike all other proteogenic amino acids forms no intramolecular hydrogen bonds between the amide hydrogen and carbonyl groups nearby (Fig. 2c and S9†). Another piece of evidence for the role of backbone N–H emanated from measurement of the rates of the Wittig reaction with di-alanine and di-Sarcosine oxaloyl aldehydes (Fig. 3c). An HCO–Sarcosine–Sarcosine aldehyde devoid of backbone N–H exhibited a 5-fold decrease in reactivity when compared to isomeric HCO–
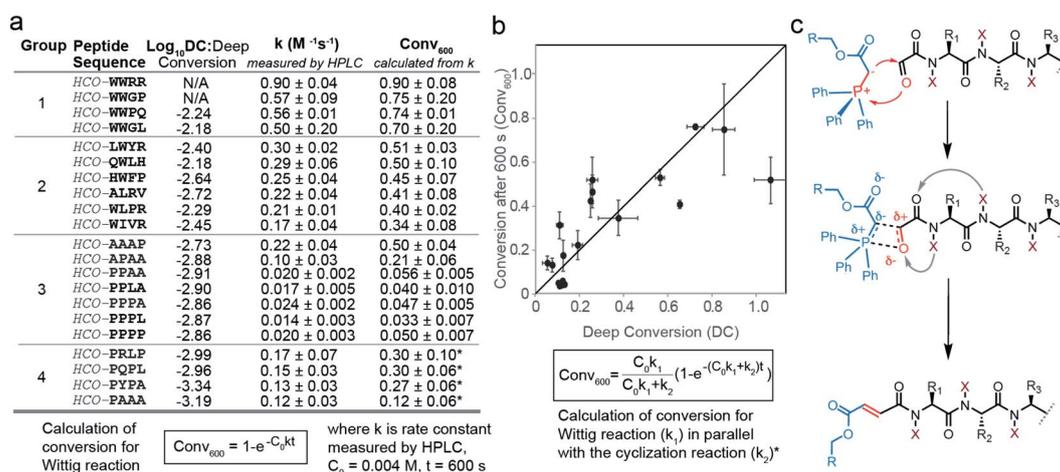

Group	Peptide Sequence	Log₁₀DC:Deep Conversion	k ($M^{-1}s^{-1}$) measured by HPLC	Conv₆₀₀ calculated from k
1	HCO–**WWRR**	N/A	0.90 ± 0.04	0.90 ± 0.08
	HCO–**WWGP**	N/A	0.57 ± 0.09	0.75 ± 0.20
	HCO–**WWPQ**	-2.24	0.56 ± 0.01	0.74 ± 0.01
	HCO–**WWGL**	-2.18	0.50 ± 0.20	0.70 ± 0.20
2	HCO–**LWYR**	-2.40	0.30 ± 0.02	0.51 ± 0.03
	HCO–**QWLH**	-2.18	0.29 ± 0.06	0.50 ± 0.10
	HCO–**HWFP**	-2.64	0.25 ± 0.04	0.45 ± 0.07
	HCO–**ALRV**	-2.72	0.22 ± 0.04	0.41 ± 0.08
	HCO–**WLPR**	-2.29	0.21 ± 0.01	0.40 ± 0.02
	HCO–**WIVR**	-2.45	0.17 ± 0.04	0.34 ± 0.08
3	HCO–**AAAP**	-2.73	0.22 ± 0.04	0.50 ± 0.04
	HCO–**APAA**	-2.88	0.10 ± 0.03	0.21 ± 0.06
	HCO–**PPAA**	-2.91	0.020 ± 0.002	0.056 ± 0.005
	HCO–**PPLA**	-2.90	0.017 ± 0.005	0.040 ± 0.010
	HCO–**PPPA**	-2.86	0.024 ± 0.002	0.047 ± 0.005
	HCO–**PPPL**	-2.87	0.014 ± 0.003	0.033 ± 0.007
	HCO–**PPPP**	-2.86	0.020 ± 0.003	0.050 ± 0.007
4	HCO–**PRLP**	-2.99	0.17 ± 0.07	0.30 ± 0.10*
	HCO–**PQPL**	-2.96	0.15 ± 0.03	0.30 ± 0.06*
	HCO–**PYPA**	-3.34	0.13 ± 0.03	0.27 ± 0.06*
	HCO–**PAAA**	-3.19	0.12 ± 0.03	0.12 ± 0.06*

Calculation of conversion for Wittig reaction

$$Conv_{600} = 1 - e^{-C_0 kt}$$

where k is rate constant measured by HPLC, $C_0 = 0.004$ M, $t = 600$ s

$$Conv_{600} = \frac{C_0 k_1}{C_0 k_1 + k_2}(1 - e^{-(C_0 k_1 + k_2)t})$$

Calculation of conversion for Wittig reaction (k_1) in parallel with the cyclization reaction (k_2)*

Fig. 2 (a) Deep conversion (DC), rate constants measured by HPLC and conversion at 600 seconds (Conv₆₀₀). Sequences marked as "N/A" in the Log₁₀ DC column were not detected in the naïve library but were predicted by bioinformatics analysis of the sequencing data, and all other sequences came from the selection. The group and order are based on families of peptide sequences. Group 1 contains fast reacting sequences that begin with WW, group 2 contains average reacting sequences ordered by the decreasing reaction rate, group 3 contains slow reacting sequences which are sorted by increased prevalence of Pro (P) (from one to two, three and four Pro residues) and group 4 contains sequences that exhibit 6-exo-trig side reactions in addition to the Wittig reaction. (b) Plot of DC vs. Conv₆₀₀. Calculations of the conversion from experimentally measured rate constants. (c) Reaction mechanism of the Wittig reaction in peptides.
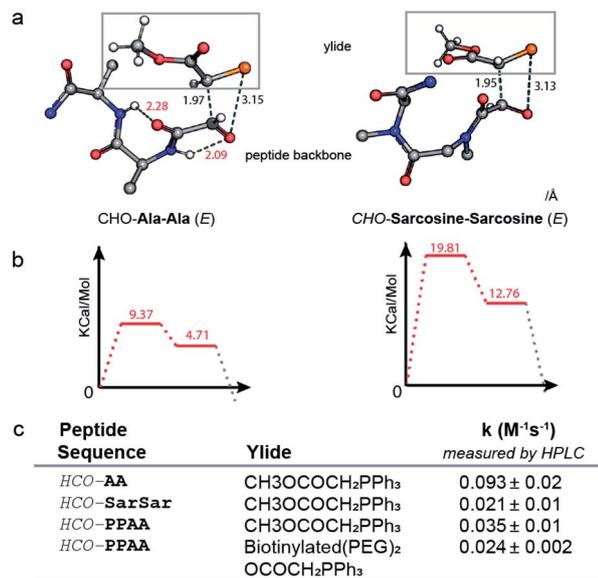
Fig. 3 (a) Geometries of E Ala–Ala and Sarcosine–Sarcosine rate determined transition states (TS1) in gas (B3LYP 6-31G(d)). First and second amides formed intramolecular hydrogen bonds and distances are labelled in red. Distances in OPA are labelled in black. (b) Energy gap of E Ala–Ala and Sarcosine–Sarcosine transition states, and TS1 is selected as the rate-limiting step. (c) Model peptide rate constants measured by HPLC.

Ala–Ala aldehyde. To test further whether backbone primary amide contributes to stabilization of the transition state, we performed DFT calculations of the transition state geometry using the Gaussian 09 software[43] and B3LYP 6-31G(d) basis set. Due to the conformational flexibility and complexity of oxyclic tetrapeptides and without access to a putative starting structure for the TS, the TS could not be located for the full tetrapeptide. On the other hand, the TS geometries of simpler model dipeptides such as HCO–Ala–Ala and HCO–Sarcosine–Sarcosine and a simple ylide $CH_3OCO(CH_2)$–P^+Ph_3 were successfully optimized using DFT; further details on the computational methods are provided in the ESI.† Similar to the previous calculations of the TS of the Wittig reaction for stabilized ylides, we observed two transition states and TS1 exhibits a higher energy barrier than TS2 (Fig. S11†).[37,38] We focused on the geometry and relative energies of TS1 to understand the preferences in the rate limiting step of these reactions. In the optimized geometry of TS1 of HCO–Ala–Ala, we observed two intramolecular hydrogen bonds between the backbone N–H and two carbonyls of the oxaloyl (Fig. 3a). The analysis shown in Fig. 3 is focused on the E-isomer of TS1 because both DFT calculations and experiments favor formation of the E Wittig product (Fig. S11†). In TS1 of HCO–Sarcosine–Sarcosine, N-methylated backbone amides were unable to form such interactions and showed 10 kcal mol^{-1} higher than the HCO–Ala–Ala TS1 (Fig. 3b). As these two TS1 have the same atomic composition, the difference in energy interactions can be neglected. Thus, the energy barrier of HCO–Ala–Ala TS1 can be attributed to the stabilization of HCO–Ala–Ala TS1 by two hydrogen bonds. Experimental measurements of the rate constants of the

reaction between HCO–Ala–Ala, HCO–Sarcosine–Sarcosine and ylide $CH_3OCOCH_2PPH_3$, corroborated the results from computations (Fig. 3c). We were also able to obtain TS1 and TS2 for HCO–Pro–Pro and HCO–Trp–Trp substrates and observed a similar role of backbone amides in TS1 (Fig. S12 and S13†).

To determine whether the change in the rate of the Wittig reaction was due to the influence of amino acid on the OPA TSs or the inherent reactivity of substrates towards any nucleophilic attack, we measured the rate of the reaction of HCO–PPAA and HCO–WWRR sequences with 2,4-dinitrophenylhydrazine. To our surprise, the reactivity for hydrazine ligation was reversed (Fig. S14 and S15†) and HCO–PPAA reacted at least 2 times faster than HCO–WWRR both at pH 0 and pH 5. These results (Fig. S16 and S17†) demonstrate that the increase in reactivity is not due to the inherent increase of the electrophilicity of the substrate but due to reaction-specific effects such as the geometry and the relative energy of the TS.

DFT calculations showed lower energies of TS1-E barriers when compared to the TS1-Z configuration for all calculated substrates (Fig. S11†). HPLC and NMR analysis confirmed that the E product was favoured over Z for HCO–Ala–Ala (E/Z 4.5 : 1) and HCO–Sarcosine–Sarcosine (E/Z 3.6 : 1) (Fig. S21 and S22†). We note that the selection process was not designed to select sequences that react stereoselectively. Still, we noticed interesting changes in E/Z selectivity in the Wittig reaction of "fast" (CHO–WWRR 1 : 1 E/Z), "medium" (CHO–HWFP 1 : 9 E/Z) and "slow" (CHO–PPAA 4.5 : 1 E/Z) reacting sequences (Fig. S18–S20†). These results provide additional evidence that the side chains of the amino acids and backbone amides might exert different influences on the E-OPA $vs.$ Z-OPA transition states.

Application to the cyclic library

Applying the conditions (10 min. reaction, 0.4 mM [YEB]) that convert 1% of the population to another library $SXCX_3C$, we found that the effect of amino-acid residues on conversion was significantly attenuated when compared to the SX_4 library (Fig. S23 and S24,† all the DC values are available in http://SXCXXXC.csv). These results were not surprising because the previous observations suggested that synergistic contributions from the amino acids at both positions 1 and 2 are critical to change the reactivity. However, in the $SXCX_3C$ library the synergy between position 1 and 2 is not possible because this library contains a constant cysteine at the second position. As in SX_4, the presence of proline in the first, but not the third position led to a decrease of DC due to proline-assisted 6-exo-trig attack of amide nitrogen on aldehyde to afford intramolecular cyclization.[42] In the $SXCX_3C$ library, tryptophan and tyrosine in the first (but not the third) position lead to a modest increase in conversion. The synthesis and testing of five sequences confirmed that the placement of Tyr in the first position led to a detectable increase in the rate (Fig. S23f†) whereas peptides with Tyr in the third position exhibited average rates similar to the average rate of peptides from the SX_4 library. Modification of the $SXCX_3C$ library was not useful for identification of new sequences with low or high reactivity; still, a uniform reactivity of such a library is an advantage. Such
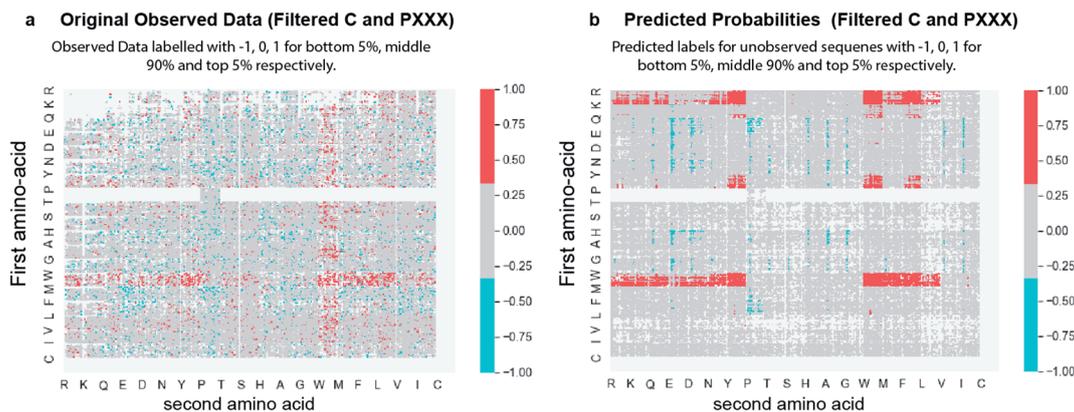
Fig. 4 (a) 20 × 20 plots showing original observed data with class labels for HIGH (top 5%), MEDIUM (middle 90%) and LOW (bottom 5%) as 1, 0, and −1 respectively. Sequences not observed experimentally are shown in white. (b) 20 × 20 plot showing the predicted labels of 99 568 non-observed sequences with 1, 0, and −1 corresponding to HIGH, MEDIUM, and LOW, respectively (Fig. S30†). 60 432 sequences from original observed data were omitted from this plot (showed as white pixels). Red points denote peptides with high probability of the 'fast' label, while blue denotes peptides with high probability of the 'slow' label. Data for PXXX sequences but not PPXX were excluded from training and predictions on purpose due to side reactions in these sequences.

a library can be considered as an example of library in which majority of the members exhibit the same reactivity towards one chemical modification.

Machine learning using DC values to predict non-observed sequences

Analysis by deep-sequencing made it possible to observe 60 432 of the 160 000 possible tetramer amino acid sequences. Measurement of the rates of the remaining 99 568 sequences was not possible for multiple reasons, such as low or unreliable count of these peptide sequences in the naïve population. We sought to extrapolate the reactivity of the "missing" 99 568 peptides using a machine learning model trained using the data from the "observed" 60 432 sequences. As a proof-of-principle, we trained a classification model. The experimentally observed data were split into 'HIGH' or 'LOW' deep conversion subgroups where HIGH and LOW are defined by the highest and lowest 5% of the DC values obtained by experimental observation (Fig. S26†). As sequences with single Pro in the first position exhibit a side-reaction, these sequences were not used for training. Using XGBoost[44] (gradient boosted decision trees) (Fig. S27†), we trained two binary classifiers: one to identify sequences belonging to the HIGH subgroup and the other to identify sequences belonging to the LOW subgroup (Fig. S28,† all the prediction probabilities are available in http://Predictions-160-Probabilities.csv). The input features included the quantitative chemical properties of each of the amino acids in the tetramer sequences, namely z-scale[45] descriptors (3 × 4 AA position = 12 features), VHSE[46] (vectors of hydrophobic, steric, and electronic properties) descriptors (8 × 4 AA position = 32 features), and sequence patterns based on permutations of 20 amino acids among 4 positions within the tetramer sequences (2396 features) to yield a total of 2440 features (more details about features can be found in the ESI† section titled "Feature Engineering"). Evaluation of respective classifiers showed the area under the receiver operating characteristic

curve (ROC AUC) scores of 81.2 ± 0.4 and 73.7 ± 0.8 for HIGH and LOW, using 5-fold stratified cross-validation. It also showed F1-scores of 33.7 ± 0.9 and 19.0 ± 0.9 for the respective classifiers (Table S4†). We deployed the learned models into a publicly available web app (http://44.226.164.95/, Fig. S29†) which allows users to compute the probability of sequences belonging to both the HIGH and LOW class. Using this model, we predicted the class labels of 99 568 amino acid sequences not observed in sequencing. Fig. 4 compares two 20 × 20 plots, one shows the experimentally measured labels for 60 432 sequences (Fig. 4a) and the other shows predicted labels for peptides never observed in deep sequencing (Fig. 4b). The learned models (Fig. 4b) suggest definitive patterns of reactivity that were not clearly observed in the scarce experimental data (Fig. 4a). 8 peptides predicted from machine learning (5 predicted fast and 3 predicted slow) were synthesized and the experimental reaction rates were tested (Table S5†). From three predicted slow peptides (sequences do not initiate with PP), all three showed slower experimental reaction rates than 6 predicted fast peptides, two were faster than the average, two exhibited average reactivity, and interestingly one exhibited a complete class switch, and the rate of the Wittig reaction of CHO–RYIP was the slowest of all tested sequences (0.003 M^{-1} s^{-1}). It is possible that the model cannot reliably predict the reactivity of motifs with N-terminal Arg because they are censored from naïve libraries.[41]

Conclusions

In conclusion, a genetically encoded library of >10^5 phage-displayed peptide aldehydes provided a rich dataset guiding SAR studies for the Wittig reaction in water with a stabilized ylide (YEB). The study highlighted the cooperative effect of the first and second N-terminal amino acids on the rate of the reaction. Low reactivity of the PP motif highlights the role of backbone amides in stabilization of the TS of the Wittig reaction. DFT

computations corroborated the experimental observations and suggested intramolecular hydrogen bonds with backbone amides as an important stabilization factor for the transition state of the Wittig reaction. The 50-fold dynamic range of the reaction rate suggested a 3 kcal mol^{-1} contribution to the Wittig TS from the peptide and a large fraction of this contribution emanates from the backbone amides.

Coupling of the deep sequencing methodology to investigation of chemical reactivity and SAR studies with only minor changes can be applied to investigate other M13 virion compatible reactions already known to be compatible with the M13 virion (thiol SN_2,[47–50] thiol SNAr,[51] oxime ligation,[32,52] copper catalyzed azide alkyne cycloaddition,[53] copper-free azide alkyne cycloaddition,[54] and Diels Alder cycloaddition[31]). These investigations, in principle would follow the same experimental design: (i) couple the reactive group to biotin; (ii) terminate the reaction at 1–5% conversion and (iii) sequence the reactive (biotinylated) population. This approach can also illustrate the SAR of other reactions that have potential to be applied on phage such as multicomponent reactions compatible with aqueous conditions[55] or chemistry that has already been explored on proteins, unprotected peptides and other display platforms[34,40,56–58] As chemical modification of DNA and RNA-displayed libraries is also possible, the SAR of reactions that modify these libraries could be investigated in a similar fashion. In principle, peptide libraries combined with calibrated mass spectrometry analysis,[59] could permit analogous SAR analysis, however, the dynamic range of the mass-spectrometry instrument should be sufficient to quantify peptides both enriched and depleted in the reaction.

The SAR data sets produced by deep-sequencing are sufficiently large for training of machine learning models. As a proof-of-principle example, we trained a classification model and attained a respectable accuracy as determined by cross-validation in a held-out dataset. Most importantly, testing of ML models has to extend beyond simple evaluation of accuracy in a cross-validation. Experimental data showed that ML predictions are more reliable on slow reacting peptides. We envision several important next steps in the application of ML approaches to such datasets: (i) replacing peptide-centric descriptors with all-atomic molecular descriptors will make it possible to extrapolate the reactivity of the non-peptide structure from a peptide dataset; (ii) training of quantitative regression models in place of classification will make it possible to predict the structure with higher or lower reactivity than any of the experimentally observed structures.

Data availability

The datasets supporting this article have been uploaded as part of the ESI.† All the MATLAB scripts are available at SupplementaryData.rar. The deep sequencing data with DNA reads, raw counts can be found in VT_unfiltered_Feb.txt, and were uploaded to http://48hd.cloud/ server with an unique alphanumeric name (e.g., 20170829-09WIooPA-VT) and an unique static URL can be found in the ESI Section 3.2.† All the Gaussian output files are available in SupplementaryData.rar/DFT calculation. Machine learning algorithm info is available at https://github.com/derdalab/GESAR.

Author contributions

V. T. performed synthesis of chemical and biochemical reagents, modification, selection, and analysis of the phage display libraries. K. Y. performed synthesis, and modification of peptides. S. M. and S.·V. K. designed and implemented the machine learning algorithm to produce the machine learned model. S. V. K. developed the prediction web app. K. Y. and K. A.-D., performed the DFT computation. R. D., V. T., K. Y. and S. M. wrote the manuscript, edited the final manuscript and contributed intellectual and strategic input. All authors approved the final manuscript.

Conflicts of interest

There are no conflicts to declare.

Acknowledgements

Notes and references

1 M. T. Reetz, *Angew. Chem., Int. Ed.*, 2002, **41**, 1335–1338.

2 L. P. Hammett, *Chem. Rev.*, 1935, **17**, 125–136.

3 T. Wang, M.-B. Wu, J.-P. Lin and L.-R. Yang, *Expert Opin. Drug Discovery*, 2015, **10**, 1283–1300.

4 C. B. Santiago, J.-Y. Guo and M. S. Sigman, *Chem. Sci.*, 2018, **9**, 2398–2412.

5 P. S. Kutchukian, J. F. Dropinski, K. D. Dykstra, B. Li, D. A. DiRocco, E. C. Streckfuss, L.-C. Campeau, T. Cernak, P. Vachal, I. W. Davies, S. W. Krska and S. D. Dreher, *Chem. Sci.*, 2016, **7**, 2604–2613.

6 A. R. Katritzky, V. S. Lobanov and M. Karelson, *Chem. Soc. Rev.*, 1995, **24**, 279–287.

7 K. C. Harper, E. N. Bess and M. S. Sigman, *Nat. Chem.*, 2012, **4**, 366–374.

8 B. A. Bunin, M. J. Plunkett and J. A. Ellman, *Proc. Natl. Acad. Sci. U. S. A.*, 1994, **91**, 4708–4712.

9 K. D. Collins, T. Gensch and F. Glorius, *Nat. Chem.*, 2014, **6**, 859–871.

10 J. A. Selekman, J. Qiu, K. Tran, J. Stevens, V. Rosso, E. Simmons, Y. Xiao and J. Janey, *Annu. Rev. Chem. Biomol. Eng.*, 2017, **8**, 525–547.

11 D. D. Devore and R. M. Jenkins, *Comments Inorg. Chem.*, 2014, **34**, 17–41.

12 G. Gasparini, M. Dal Molin and L. J. Prins, *Eur. J. Org. Chem.*, 2010, **2010**, 2429–2440.

13 M. T. Reetz, *Angew. Chem., Int. Ed.*, 2001, **40**, 284–310.

14 M. T. Reetz, *Angew. Chem., Int. Ed.*, 2008, **47**, 2556–2588.

15 D. W. Robbins and J. F. Hartwig, *Science*, 2011, **333**, 1423–1427.

16 Y. Maeda, O. V. Makhlynets, H. Matsui and I. V. Korendovych, *Annu. Rev. Biomed. Eng.*, 2016, **18**, 311–328.

17 X. Gao and H. B. Kagan, *Chirality*, 1998, **10**, 120–124.

18 C. Gennari, S. Ceccarelli, U. Piarulli, C. A. G. N. Montalbetti and R. F. W. Jackson, *J. Org. Chem.*, 1998, **63**, 5312–5313.

19 H. Kim, G. Gerosa, J. Aronow, P. Kasaplar, J. Ouyang, J. B. Lingnau, P. Guerry, C. Farès and B. List, *Nat. Commun.*, 2019, **10**, 770.

20 M. R. anderHeiden, H. Plenio, S. Immel, E. Burello, G. Rothenberg and H. C. J. Hoefsloot, *Chem.–Eur. J.*, 2008, **14**, 2857–2866.

21 T. Satyanarayana, S. Abraham and H. B. Kagan, *Angew. Chem., Int. Ed.*, 2009, **48**, 456–494.

22 M. W. Kanan, M. M. Rozenman, K. Sakurai, T. M. Snyder and D. R. Liu, *Nature*, 2004, **431**, 545–549.

23 M. M. Rozenman, M. W. Kanan and D. R. Liu, *J. Am. Chem. Soc.*, 2007, **129**, 14933–14938.

24 Y. Chen, A. S. Kamlet, J. B. Steinman and D. R. Liu, *Nat. Chem.*, 2011, **3**, 146–153.

25 K. D. Hook, J. T. Chambers and R. Hili, *Chem. Sci.*, 2017, **8**, 7072–7076.

26 A. I. Chan, L. M. McGregor and D. R. Liu, *Curr. Opin. Chem. Biol.*, 2015, **26**, 55–61.

27 F. Tanaka, R. Fuller, L. Asawapornmongkol, A. Warsinke and S. Gobuty, *Bioconjugate Chem.*, 2007, **18**, 1318–1324.

28 G. M. Eldridge and G. A. Weiss, *Bioconjugate Chem.*, 2011, **22**, 2143–2153.

29 R. K. V. Lim, N. Li, C. P. Ramil and Q. Lin, *ACS Chem. Biol.*, 2014, **9**, 2139–2148.

30 B. N. Tse, T. M. Snyder, Y. Shen and D. R. Liu, *J. Am. Chem. Soc.*, 2008, **130**, 15611–15626.

31 V. Triana and R. Derda, *Org. Biomol. Chem.*, 2017, **15**, 7869–7877.

32 S. Ng, M. R. Jafari, W. L. Matochko and R. Derda, *ACS Chem. Biol.*, 2012, **7**, 1482–1487.

33 S. Ng, K. F. Tjhung, B. M. Paschal, C. J. Noren and R. Derda, in *Peptide Libraries: Methods and Protocols*, ed. R. Derda, Springer New York, New York, NY, 2015, pp. 155–172.

34 S. Ng, M. R. Jafari and R. Derda, *ACS Chem. Biol.*, 2012, **7**, 123–138.

35 L. Wang, A. Brock, B. Herberich and P. G. Schultz, *Science*, 2001, **292**, 498–500.

36 I. S. Carrico, B. L. Carlson and C. R. Bertozzi, *Nat. Chem. Biol.*, 2007, **3**, 321–322.

37 R. Robiette, J. Richardson, V. K. Aggarwal and J. N. Harvey, *J. Am. Chem. Soc.*, 2005, **127**, 13468–13469.

38 R. Robiette, J. Richardson, V. K. Aggarwal and J. N. Harvey, *J. Am. Chem. Soc.*, 2006, **128**, 2394–2409.

39 P. A. Byrne and D. G. Gilheany, *Chem. Soc. Rev.*, 2013, **42**, 6670–6696.

40 C. P. Ramil and Q. Lin, *Chem. Commun.*, 2013, **49**, 11007–11022.

41 B. He, K. F. Tjhung, N. J. Bennett, Y. Chou, A. Rau, J. Huang and R. Derda, *Sci. Rep.*, 2018, **8**, 1214.

42 K. Rose, J. Chen, M. Dragovic, W. Zeng, D. Jeannerat, P. Kamalaprija and U. Burger, *Bioconjugate Chem.*, 1999, **10**, 1038–1043.

43 M. J. Frisch, G. W. Trucks, H. B. Schlegel, G. E. Scuseria, M. A. Robb, J. R. Cheeseman, G. Scalmani, V. Barone, B. Mennucci, G. A. Petersson, H. Nakatsuji, M. Caricato, X. Li, H. P. Hratchian, A. F. Izmaylov, J. Bloino, G. Zheng, J. L. Sonnenberg, M. Hada, M. Ehara, K. Toyota, R. Fukuda, J. Hasegawa, M. Ishida, T. Nakajima, Y. Honda, O. Kitao, H. Nakai, T. Vreven, A. Montgomery Jr, J. E. Peralta, F. Ogliaro, M. Bearpark, J. J. Heyd, E. Brothers, K. N. Kudin, V. N. Staroverov, R. Kobayashi, J. Normand, K. Raghavachari, A. Rendell, J. C. Burant, S. S. Iyengar, J. Tomasi, M. Cossi, N. Rega, J. M. Millam, M. Klene, J. E. Knox, J. B. Cross, V. Bakken, C. Adamo, J. Jaramillo, R. Gomperts, R. E. Stratmann, O. Yazyev, A. J. Austin, R. Cammi, C. Pomelli, J. W. Ochterski, R. L. Martin, K. Morokuma, V. G. Zakrzewski, G. A. Voth, P. Salvador, J. J. Dannenberg, S. Dapprich, A. D. Daniels, Ö. Farkas, J. B. Foresman, J. V. Ortiz, J. Cioslowski and D. J. Fox, *Gaussian 09 (Revision A.02)*, Gaussian, Inc., Wallingford CT, 2016.

44 T. Chen and C. Guestrin, *Proceedings of the 22nd acm sigkdd international conference on knowledge discovery and data mining*, 2016, pp. 785–794.

45 C. Ge, E. Spånning, E. Glaser and Å. Wieslander, *Mol. Plant*, 2014, **7**, 121–136.

46 J. Xie, Z. Xu, S. Zhou, X. Pan, S. Cai, L. Yang and H. Mei, *PLoS One*, 2013, **8**, e74506.

47 S. Li and R. W. Roberts, *Chem. Biol.*, 2003, **10**, 233–239.

48 M. R. Jafari, L. Deng, P. I. Kitov, S. Ng, W. L. Matochko, K. F. Tjhung, A. Zeberoff, A. Elias, J. S. Klassen and R. Derda, *ACS Chem. Biol.*, 2014, **9**, 443–450.

49 S. Chen, J. Morales-Sanfrutos, A. Angelini, B. Cutting and C. Heinis, *ChemBioChem*, 2012, **13**, 1032–1038.

50 S. Ng and R. Derda, *Org. Biomol. Chem.*, 2016, **14**, 5539–5545.

51 S. Kalhor-Monfared, M. R. Jafari, J. T. Patterson, P. I. Kitov, J. J. Dwyer, J. M. Nuss and R. Derda, *Chem. Sci.*, 2016, **7**, 3785–3790.

52 Z. M. Carrico, M. E. Farkas, Y. Zhou, S. C. Hsiao, J. D. Marks, H. Chokhawala, D. S. Clark and M. B. Francis, *ACS Nano*, 2012, **6**, 6675–6680.

53 F. Tian, M.-L. Tsao and P. G. Schultz, *J. Am. Chem. Soc.*, 2004, **126**, 15962–15963.

54 T. Urquhart, E. Daub and J. F. Honek, *Bioconjugate Chem.*, 2016, **27**, 2276–2280.

55 M. C. Pirrung and K. D. Sarma, *J. Am. Chem. Soc.*, 2004, **126**, 444–445.

56 R. J. Spears and M. A. Fascione, *Org. Biomol. Chem.*, 2016, **14**, 7622–7638.

57 R. A. Goodnow, C. E. Dumelin and A. D. Keefe, *Nat. Rev. Drug Discovery*, 2017, **16**, 131–147.

58 J. R. Frost, J. M. Smith and R. Fasan, *Curr. Opin. Struct. Biol.*, 2013, **23**, 571–580.

59 C. Zhang, M. Welborn, T. Zhu, N. J. Yang, M. S. Santos, T. Van Voorhis and B. L. Pentelute, *Nat. Chem.*, 2016, **8**, 120–128.